

Twin inclined jets in crossflow: experimental investigation of different flow regimes and jet elevations

A. Radhouane¹ · N. Mahjoub Saïd² · H. Mhiri¹ ·
Ph. Bournot³ · G. Le Palec³

Received: 11 August 2014 / Accepted: 13 April 2015 / Published online: 19 April 2015
© Springer Science+Business Media Dordrecht 2015

Abstract The present experimental study is dedicated to unfolding the mixing process generated by double-inclined, variably elevated jets in crossflow. Twin tandem jets in crossflow are very common in the industry and are closely dependent on several parameters. Detailing the induced interactions in such a model would ultimately enhance our understanding and help optimize related applications. The jets handled in the present work are placed three diameters apart, arranged in line with the oncoming crossflow and sent at variable levels ($h = 0, 1, 2, 5$ cm) from the ground of a wind tunnel and are discharged from elliptic discharging cross sections. Elliptic jets are of particular interest in applications like industrial and boat chimneys, and are practically easily obtained by razing circular cylinders at the desired inclination and height. Particle image velocimetry and coupled charge device CCD camera were used. The dynamic and turbulent behavior of the resulting flowfield was characterized in terms of streamlines, velocity components and vortical structures. The obtained data helped highlight the impact of jets' elevation over their mixing mechanism among the surrounding free stream: establishment of the resulting flowfield dynamics and settlement of the induced vortical structures. The mixing process evolution was also considered under different flow regimes. For the matter an injection ratio (defined as jets to the mainstream's velocity ratio) raging between 0.67, 1 and 1.29 was considered. These cases correspond to jets dynamically dominated by, equivalent to or more dominant than the mainstream. The impact of jets' elevation combined to that of the injection ratio affects both the developed vortical structures and the established dynamic fields, which in turn highly affects the induced mixing process.

Keywords Twin jets · Crossflow · Jets' elevation · Injection rate · Dynamic mixing process

✉ N. Mahjoub Saïd
mahjoub_nejla@yahoo.fr; Nejla.mahjoub@fsm.rnu.tn

¹ TTPI, National Engineering School of Monastir, University of Monastir, Monastir, Tunisia

² LGM, National Engineering School of Monastir, IPEIM, University of Monastir, Monastir, Tunisia

³ IUSTI, UMR 7343, Faculty of Science, University of Aix-Marseille, Marseille, France

List of symbols

d	Jet nozzle diameter (m)
D	Nozzles' spacing (m)
f	Mass fraction
h	Jet's height (m)
k	Kinetic energy of turbulence (m^2/s^2)
R	Velocity ratio
T	Temperature (K)
U_∞	Crossflow velocity (m/s)
V_0	Injection velocity (m/s)
u, v, w	Velocity components along $x, y,$ and z directions (m/s)
x, y, z	Cartesian coordinates (m)

Greek symbols

ε	Dissipation rate of the turbulent kinetic energy
α	Injection angle ($^\circ$)

Subscripts

∞	Conditions in crossflow
0	Exit section of the jet

Superscripts

\sim	Favre average
--------	---------------

1 Introduction

Twin jets in crossflow are involved in several industrial applications and have serious repercussions on the environment. Rising levels of vehicle exhaust and chimney stack fumes in the atmosphere and the dumping of liquid effluents in streams and rivers have a direct impact on the environment. Mixing quality of jets in crossflow in combustion and chemical processing industries, however, has an indirect impact on the environment. A low quality of mixing causes temperature fluctuations, which in turn leads to higher NO_x emissions. The correlation between the temperature peaks and the production of pollutants, namely NO_x , was proven by Lefebvre [1], who provided the lean premix, prevaporize (LPP) concept as a viable solution to control both parameters (temperature peaks and pollutants' production). A clear understanding of the mixing process is then crucial for an efficient reduction of turbine gas emissions.

In the field of aerospace, double jets in crossflow were examined in order to provide aircraft with better vertical/short take off and landing (V/STOL) capabilities. They were also optimized to control thrust vectors in rockets and to maneuver vehicles like aircraft and submarines.

Twin and more generally multiple jets in crossflow are involved in heat transfer applications as well. In fact, injected normally or obliquely to a wall, the emitted jets maintain the target wall at a proper temperature during high temperature thermal processes. This function is also found in the cooling process of combustors' walls and gas turbine blades. During such processes, the emitted jets are used to enhance the performance of each individual jet further downstream of its injection point [2].

The diversity of applications involving double jets in crossflow and the number of the related parameters (injection rate, nozzles' height, arrangement, inclination and cross section shape, jets' temperature and composition, etc.) generated extensive literature. Nevertheless, more research papers were dedicated to single and multiple jet configurations, in spite of the increasing pertinence of the transitional double jet model.

Consideration of this particular configuration, namely twin jet in crossflow, goes back to the early seventies when it was first examined by Ziegler and Wooler [3] by means of a physically elaborated model. The handled jets were sent normal and inclined (at 60°) to the crossflow and were arranged differently with reference to the surrounding crossflow: side by side (perpendicular to the direction of crossflow), in-line/tandem (parallel with the direction of crossflow) and off-axis/staggered (where one jet is partially shielded by the other from the crossflow). Jet trajectories were tracked for a jet to crossflow ratio equal to 8 and a variable jet spacing distance. The deflection of the emitted jets was explained by means of pressure gradient while the entrainment and the effect of each jet on the other were dynamically specified.

Further studies examined the different twin jets' arrangements; namely tandem, side by side and staggered. Investigation was carried out simultaneously and contrasted with models with a variable number of emitted jets. Early studies were more comprehensive as they provided comparison references for both single and multiple jet models [4, 5]; whereas recent studies were more focused as twin models; under their different arrangements; were exclusively compared to single jet models [6–9].

Ziegler and Wooler [3] pioneered such comparative studies of differently arranged twin jets in crossflow towards both single and multiple jet cases [4]. Comparisons were based on velocity stratification procedures, which consist in constructing equivalent nozzles with similar mass flow and thrust but having a uniform exit velocity profile.

Three differently stratified-velocity single jets were considered: jets with a relatively high velocity core, jets with a relatively low velocity core and jets originating from a vaned nozzle. Procedures proved to be well representative in all cases with reference to test data. An alternative procedure was further developed for the cases of the vaned and low velocity core nozzles and validated with reference to the same test data, in terms of internal mixing, jet centerlines and induced surface static pressures.

Jets were set later in pairs according to different arrangements: tandem, side by side and staggered. Mutual interference and jet blocking effects were thoroughly evaluated, and in each case the equations were checked, suited to the configurations and validated by the test data.

Similarly, Gregoric et al. [5] compared the merging process of twin buoyant jets in crossflow at their different possible arrangements (tandem side by side and staggered) to the mixing process induced by single and multiple jets in crossflow. The comparison was carried out experimentally and included the injection ratio (0.2, 0.5 and 1.0) as an extra evaluation parameter. Results were based on fluorescent-dye-visualizations and a vertical slit light source. They provided heights, widths, and vertical cross sections of the deflected jets in an attempt to characterize the induced entrainment. Special interest was given to the horseshoe shape of the cross sections as well as to the trailing vortex sheet developed in the jet wakes. It showed that an increasing number of discharging jets in a staggered arrangement remarkably decreased the amount of entrainment.

The second category of surveys available in the literature and dealing with the different possible arrangements of twin jet models (tandem, side by side and staggered) are more detailed and focused, as already mentioned [6–9] since they were mainly compared to single jet models in terms of rise and shape of air and/or water plumes. Macdonald et al. [6]

first adopted this strategy by considering the dispersion of twin elevated jets in a water tunnel. Injection ratio, jets' density, the stack separating distance and of course jets' arrangement were varied, at a 1/500 scale. This led to a comprehensive analysis of jets' rise and additional rise rates in addition to a consistent description of plumes' structures. A decreasing stack distance combined with an inline arrangement resulted in an enhanced additional rise, close to or even above the maximum theoretical rise enhancement factor (equivalent to 2^1). This factor decreased in an oblique arrangement and tended towards zero when side by side orientation was reached. In fact, side-by-side jet's merge is closely dependent on the reorganization of the separate plumes' buoyancy [reorganization through destructive interactions between the nearby counter rotating vortex pairs (CVPs)]. As each vortex opposes the other, a downwash effect is generated, justifying the absence of any additional rise.

Single and differently arranged twin jet models were further experimented by Contini and Robins [7] and Contini et al. [8], in the case of air jets and crossflow. In addition to jets' orientation, Contini and Robins [7] evaluated the impact of the stack distance over plume trajectories and shape of the jet cores, documenting crossflow's entrainment. The corresponding plume-visualization and point-concentration data characterized the mixing process in terms of vorticity and concentration distributions, quantifying the additional/enhanced rise of the merging jets. In a subsequent work, Contini et al. [8] restrained the number of variable parameters by considering a given jets' separating distance to concentrate more closely on the dynamic and turbulent behavior of the resulting flowfield. Fast flame ionization detectors (FFIDs) and two-component laser Doppler anemometry provided average and fluctuating concentration fields, including turbulent (vertical and longitudinal) mass fluxes. Once processed, concentration fields allowed to characterize plume trajectories, additional plume rise and concentration distributions, in the presence of both laminar and turbulent crossflows. Plume trajectories highlighted the interactions of the counter rotating vortex pairs and allowed to quantify the enhancement rise. Average and fluctuating concentration fields were analyzed quantitatively (magnitude and sign) and qualitatively by correlating it to CVPs' interactions, mixing speed and material transport. Both analyses showed that using of a gradient transport model better describes the dispersion mechanism.

Still in the context of comparisons of differently arranged twin jets versus single jets in crossflow, Kolar & Savory [9] made a survey of recent works with a special focus on velocity field and mixing process. Vorticity aspects were discussed (magnitude, associated flow structures and circulation) and correlated to the dispersion process (determined through concentration measurements [8]) under different jet separating distances and for jets emitted within both water and wind tunnels. Jets were placed flush with the ground in wind tunnels and elevated in water tunnels. Visualizations were carried out by hot wire anemometry and planar laser induced fluorescence techniques, respectively. The measured data enabled to specify the different CVPs' interaction steps: development and cancellation. They also determined their possible origins (merging process and inner vortices) and established their role in crossflow's entrainment.

However, none of the above mentioned papers evaluated the impact of the double jets' height over their interactions within the surrounding flow. It is true that Kolar and Savory [9] considered both elevated and flush-to-ground jets. Nevertheless, high jets were discharged in a water tunnel and short jets in a wind tunnel, thereby excluding any possible comparison. Some experimental attempts to assess jet's height effect are however available in the literature under specific arrangements. These attempts are attributed to Anfossi et al. [10], Gangoiiti et al. [11] and Bunsirisert et al. [12]. The variation of jets' height did not

necessarily include the case of jets emitted flush with the ground. This case was examined only by Bunsirisert et al. [12] in a side-by-side arrangement.

Moreover, considered in a specific arrangement, twin variably elevated jets were either considered [12] exclusively or compared to single [10] or both single and multiple jet models [11]. In the case of Anfossi et al. [10] and Gangoiti et al. [11], consideration was given to large scale jets in crossflow in power plants' stacks, located respectively at La Spezia gulf in the Northern Tyrrhenian Sea, and at both oil and coal fired power plants in La Coruña in Spain. As to Bunsirisert et al. [12], they considered small scale replica of double jets in crossflow, placed two diameters apart and responding to an injection ratio and a Reynolds number respectively equivalent to 3.3 and 6200.

Attention was given in three papers [10–12] to the dynamic character of the resulting flowfield. Bunsirisert et al. [12] were concerned with the induced vortical structures and jet wakes as well as their contribution to the counter rotating vortex (CVP) generation; while other research [10, 11] focused rather on jets' merge and rise processes. In the work carried out by Anfossi et al. [10], for example, the main purpose was to establish a new model based on "virtual" stack concept, likely to provide estimates of the maximum plume height. Validation was done against two semi-empirical models of Briggs, relative to similar heights and emissions [13, 14], a series of data quoted by Briggs [13] and experimental data relative to differently high stacks. A further comparison with the empirical expression of Montgomery et al. [15] enhanced the new model by bringing a correction factor for ground level concentrations in the multiple sources' case.

Double tandem jets' merge and rise processes in crossflow were further detailed experimentally by Gangoiti et al. [11]. Elaborated as part of the European project Regional Cycles of Air Pollution in the Mediterranean Area (RECAPMA), the resulting model dealt with complex atmospheric profiles-wind shear and thermal stratification in order to account for rise and dispersion processes. The handled jets contained a mixture of four components consisting of dry combustion gas, dry air, water vapor and liquid water. Once verified experimentally, plume rise prediction models were further examined. They revealed effects like plume merger in a multiple source, condensation and re-evaporation, rise in turbulent winds, rise in light winds and in stratified atmosphere with wind shear.

In light of these extensive studies, we can deduce three main points:

- Different arrangements of the double jet in crossflow model were considered, separately and/or together, and were compared or not to single and/or multiple jet models. It is worth mentioning that studies dedicated exclusively to twin tandem jets in crossflow are scarce [3], apart from some recent attempts attributed to Radhouane et al. where attention was devoted to effects of inclination and temperature [16–19].
- More attention was paid to the dynamics of the interacting flows, in terms of velocity distribution at the expense of their thermal behavior. The most frequently discussed points are related to jets' merge, rise and induced vortical structures. Nevertheless, the origin of interfering mechanisms and the induced vortices are still under study.
- The impact of double jets' elevation on their dynamics was somehow neglected, as only three papers dealing with the topic are found in the literature [11–13]. Literature discussing the effect of jets' height is by far more abundant in the case of single jets in crossflow: Moor [20], Goyal and Rama Krishna [21], Cutler [22], Rama Krishna et al. [23], Stathopoulos et al. [24], Hassan and Kelso [25], Cutler

and Kelso [26], Olcese and Toselli [27], Megerien et al. [28], Koklu and Baysal [29], Karagozian [30], etc.

Since papers exclusively dedicated to double inline jets in crossflow's model are scarce, we propose to dedicate the present experimental study entirely to it. Jets will not be discharged perpendicularly to mainstream, as in most papers but streamwise, according to an inclination angle of 60° , the inclination factor being decisive to ensure the applications' efficiency.

Isothermal cases were considered in order to focus on the dynamics of the resulting flowfield. Flow dynamics will be specified in terms of the distribution of velocity components in a first step. In a following step, we propose to further detail the resulting flowfield by exploring its turbulent behavior which was not extensively covered in the literature. This behavior will be specified in terms of vorticity fields, turbulent intensity distribution and induced vortical structures.

Herein we have to point out that all these features will be examined under a variable jet nozzle height in order to determine the role of this parameter over the jets' rise, progression and mixing within the surrounding mainstream. Different injection ratios, and then different flow regimes, are also to be considered to get a clearer idea about the impact of the injection level over the resulting flowfield in each given case.

2 Experimental setup and measurement technique

Experiments were carried out in a wind tunnel using coupled charge device (CCD) images together with two dimensional particle image velocimetry (PIV) diagnostics to obtain qualitative and quantitative measurements of the flowfield.

2.1 Wind tunnel and jets' arrangement

Twin jets in crossflow (TJICF) tests were conducted in a wind tunnel at the IUSTI, "Institut Universitaire des Systèmes Thermiques Industriels" (the university institute of industrial thermal systems), a joint research unit between the University of Provence (Aix-Marseille) and the Mediterranean University, in Marseille, France.

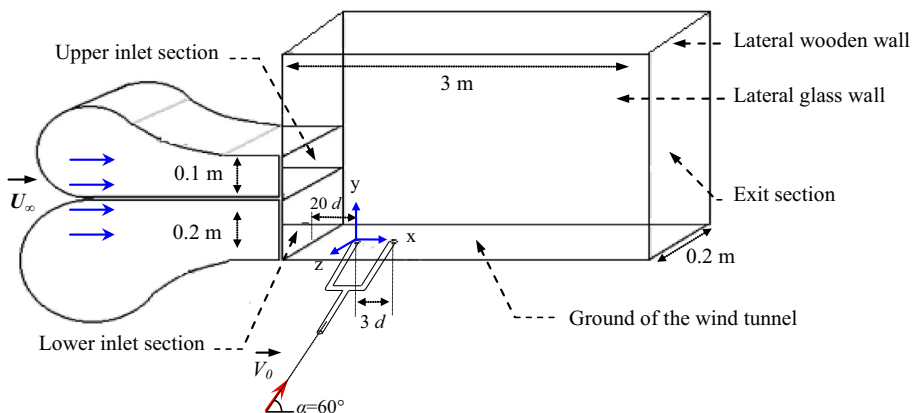


Fig. 1 Experimental setup associated Cartesian coordinate system

The wind tunnel working section measures 0.2 m wide \times 0.3 m high (20 d \times 30 d) in cross-section and is approximately $L = 3$ m (300 d) long, where d is the jets' diameter. The tunnel's dimensions, the jet nozzles' location, the orientation of the different interacting flows and the corresponding details are presented in Fig. 1.

This inlet working section is composed of two separate and independent test-sections, fed by two independent engines. The lower inlet section is 0.2 m high and the corresponding engine provides an inlet velocity ranging between 0 and 16 m/s. The upper inlet section is 0.1 m high, and the corresponding engine provides an inlet velocity ranging between 0 and 42 m/s. Since we intend to introduce a limited range of velocities, not beyond 10 m/s, we will only use the lower inlet section.

The top wall of the tunnel is open and the ground is made of wood and covered with plastic to ensure optimal visibility. One of the side walls is made of wood and painted black to prevent possible light reflexions. The second side is made of plexiglas to allow better visibility, and therefore better flow visualisations and data measurements.

The outlet section of the wind tunnel discharges directly into the atmosphere while the inlet one contains a diffuser. For better convenience during the experiments, we chose to remove the diffuser. The sudden change in the diameter is likely to affect the flow dynamics. Accordingly, we made several hot wire velocity measurements at the entrance zone of the wind tunnel in order to make sure that we were in the Reynolds independent zone. That's why we placed the rear jet nozzle approximately $0.2 \text{ m} = 20 \text{ d}$ farther from the wind tunnel entrance. This set up proved to be efficient. In fact, the mainstream velocities depicted by hot wire anemometry revealed a shear layer whose width did not exceed 10 mm (Fig. 2) and a global turbulence intensity level lower than 0.2 %.

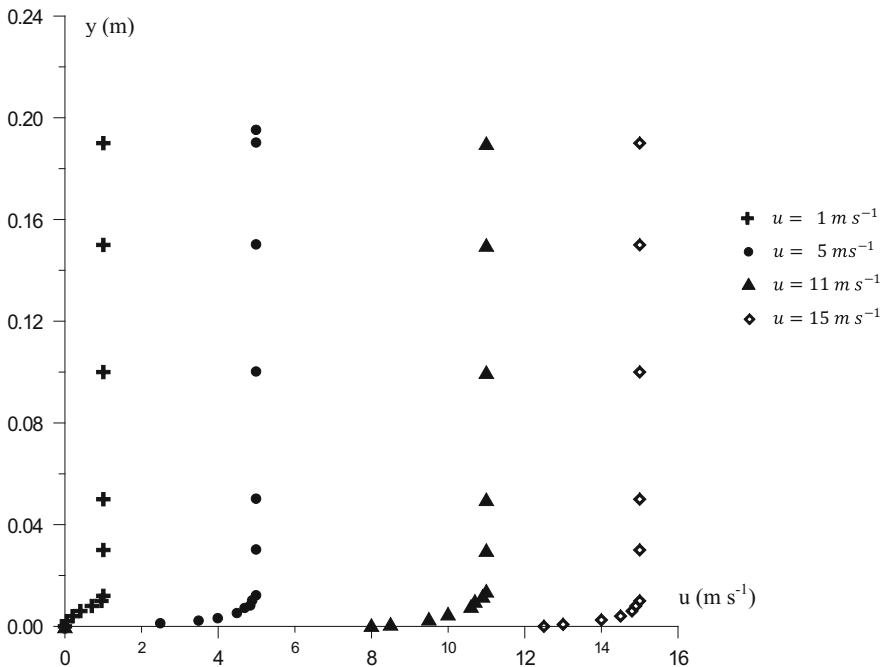


Fig. 2 Velocity profiles of the main flow at the entrance of the test section (20 cm from the entrance)

The second jet nozzle is placed three diameters downstream of the upstream one, along the centerline of the tunnel, in line with the oncoming crossflow's direction. Both jets were produced by means of two similar smooth pipes characterized by an external and an internal diameter, respectively equivalent to 12 and 10 mm (d). Pipes were first inclined according to a 60° inclination angle (α) with reference to crossflow's direction and then razed at different levels (h) from the tunnel's ground. Jets presented in Fig. 1 are placed flush with the tunnel ground. This is the initial and reference case, on which future variations (mainly concerning nozzles' height) are to be made. Once razed, jet nozzles give rise to twin elliptic tandem jets, with a longitudinal big diameter and a lateral small diameter respectively equivalent to $d/\sin \alpha$ and d .

It has to be noted that both the jets and the mainstream are fed with air, at room temperature (T_∞).

Since our ultimate goal is to evaluate the impact of the jet nozzles' height over the dynamics of the resulting flowfield, four nozzle heights were tested, $h = 1, 2$ and 5 cm, together with the reference case where jets are emitted flush to ground ($h = 0$ cm). Tests were carried out under different flow regimes, defined by different jet to mainstream velocity ratios (also called injection ratios). The tested ratios are 0.67, 1 and 1.29, and

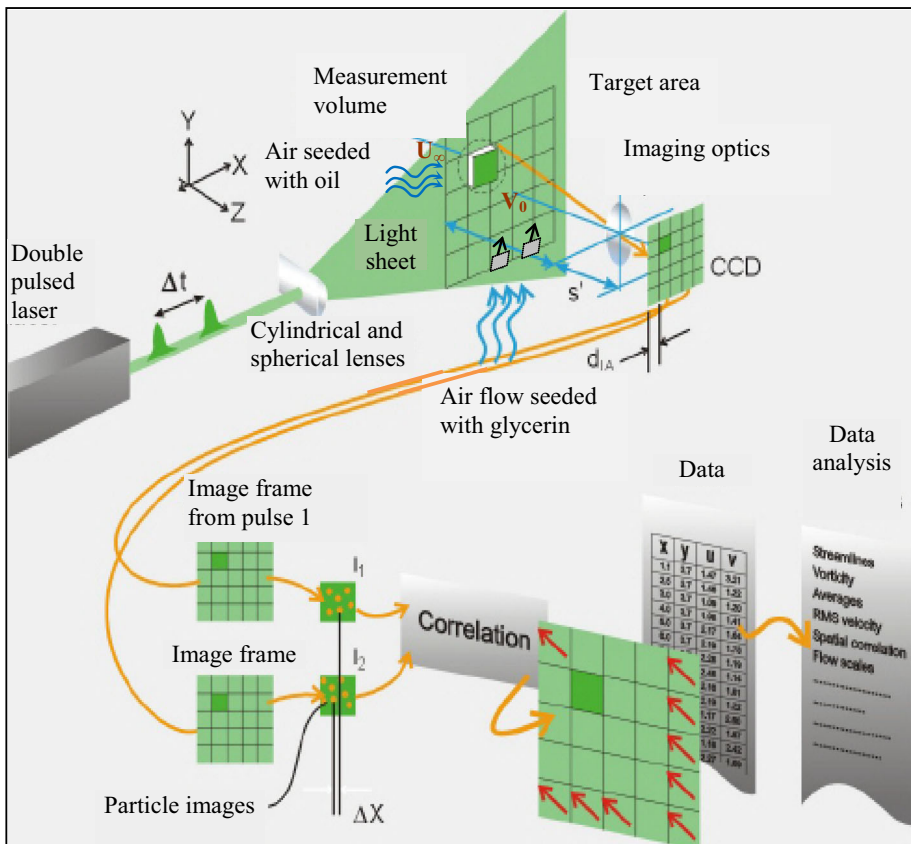


Fig. 3 PIV technique: scheme principle

correspond to jets respectively stronger than, equivalent to or weaker than the mainstream in terms of velocity and then dynamic potential to resist to the surrounding flow.

To better characterize the interacting flows and the corresponding features, we adopted the Cartesian coordinate system with an origin placed at the upstream jet nozzle centre. The choice of such a coordinate system was motivated by the asymmetry of the resulting flowfield in spite of the symmetry of the geometry as previously proved by several authors like Smith and Mungal [31], Muppidi and Mahesh [32], Yuan and Street [33], etc.

Once geometry built, and both jets and main air flows discharged, we proceeded to measurements.

2.2 Particle image velocimetry (PIV)

Several methods are used in wind tunnel experiments to quantify the features of a given flowfield, such as air flow direction, pressure and velocity as well as aerodynamic forces. In the present work, we used a Power View 4 M high resolution cross-correlation CCD (couple-charged digital) camera ($2k \times 2k$ resolution, 12 bits) to capture raw, instantaneous images of the particle-illuminated flowfield. Once collected, the images were processed by the particle image velocimetry (PIV) technique in order to provide measurements of the different characterizing features.

The PIV is a non-intrusive, laser-optical- measurement technique able to visualize and calculate instantaneous and mean dynamic fields (velocity, vorticity, turbulent intensity, etc.). It is used here to provide measurements at the xy -centre plane of the TJICF (Twin Jets In Crossflow).

The PIV is essentially based on a TSI Power View system. It consists of synchronization hardware for controlling the laser and camera, and software running on a Windows-based platform for data acquisition, management and post-analysis (Fig. 3).

Synchronization hardware includes a 50 mJ/pulse dual Nd: YAG (Neodym: Yttrium-Aluminium-Garnet) laser that produces two flat pulses at a wavelength $\lambda = 532$ nm at pulse rate of 15 Hz, the duration of each pulsation ranging from 5×10^{-9} to 10^{-8} s.

The laser is fitted with a combination of optic lenses that act together to produce a thin and focusable high intensity light sheet. These optics consist of two spherical lenses and one cylindrical lens. The cylindrical lens enables the laser beam to extend in one direction. The focal length of this cylindrical lens determines the height or the spread angle of the light sheet. As to the spherical lenses, they normally direct the laser beam at a downstream location. Focusing the light sheet, or locating the thinnest part or waist is achieved by changing the distance between the two spherical lenses. The combination of both types of lenses allows controlling the width and divergence of the generated light sheet. The intensity of the generated light depends on the power of the used laser, the dimensions of the laser beam and the width of the light sheet. Increasing the beam's dimensions enlarges the target area (area of study) but may reduce the light intensity per surface unit, which in turn may strongly affect the quality of the captured images.

Once installed, the spatial distribution of the illumination system was maintained for all subsequent tests.

Since both the jets and the crossflow are fed with air, it could be difficult to distinguish the proper progression of each flow. To sort out this problem, we seeded both flows with different tracing particles (different densities). According to Jovanovic [34], a suitable seeding for PIV measurements should be harmless to the examined flows, with a homogeneous flow spread, light scattering efficiency and minimal velocity lag. The non-perturbing character lies on the assumption that the influence of tracer particles on the fluid is

negligible. This is valid when the diameter of the tracer particles is much smaller than the typical length scale of the flow and when the difference in density is small enough. Selecting the seeding particles is then a compromise between the signal amplitude and the particles' ability to follow the flow. In fact, larger particles will increase signal quality and data rate and reduce demand for illumination, but will have a slip in accelerating flows. On the contrary, smaller particles will reduce signal amplitude and data rate and increase demand for illumination, but will follow the flow up to higher frequencies. The density of the seeding particles should also be close to that of the working fluid in order to be considered almost neutrally buoyant in the measurement area. To meet all these requirements, jets were seeded with glycerin particles with an approximate diameter of $1\ \mu\text{m}$, leading to a seeding density of approximately 30 particles per ml of pure jet fluid. The main air flow was seeded with oil droplets with an approximate diameter of $0.8\ \mu\text{m}$.

The seeding process is fully described in the circuit sketch presented in Fig. 4. The flowmeter helps regulate the flow rate of the seeding particles while the decantation reservoir is used to retain eventual contaminants present within the discharged jets. Vanes are used to control flow rates of each of the discharged jets even though similar flow rates are used in the present study.

“Insight 3G” Windows-based software from TSI Inc. was used for data acquisition, management and post-analysis. The software synchronizes pulsations according to observed phenomena and adjusts the time lapse between two images (that was $70\ \mu\text{s}$ in our case).

To avoid errors, velocity vectors were calibrated at $130\ \mu\text{m}/\text{pixel}$ and limited to the representation of the velocity field in the areas where the luminance was quite strong. The final average and turbulence velocity fields were calculated over 100 successive acquisitions. For each point, experimental uncertainties were estimated as follows: $\frac{V_{\text{max}} - V_{\text{min}}}{V_{\text{av}}}$, where

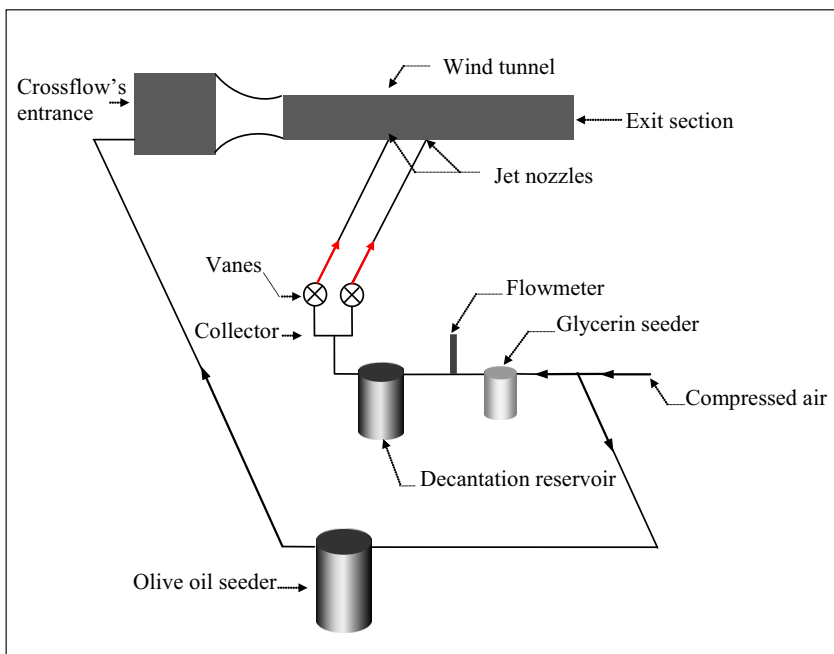


Fig. 4 Scheme of the seeding circuit

V_{max} , V_{min} and V_{av} are, respectively, the maximum velocity, the minimum velocity and the average velocity measured over the whole process. This uncertainty rate may be accounted for as follows:

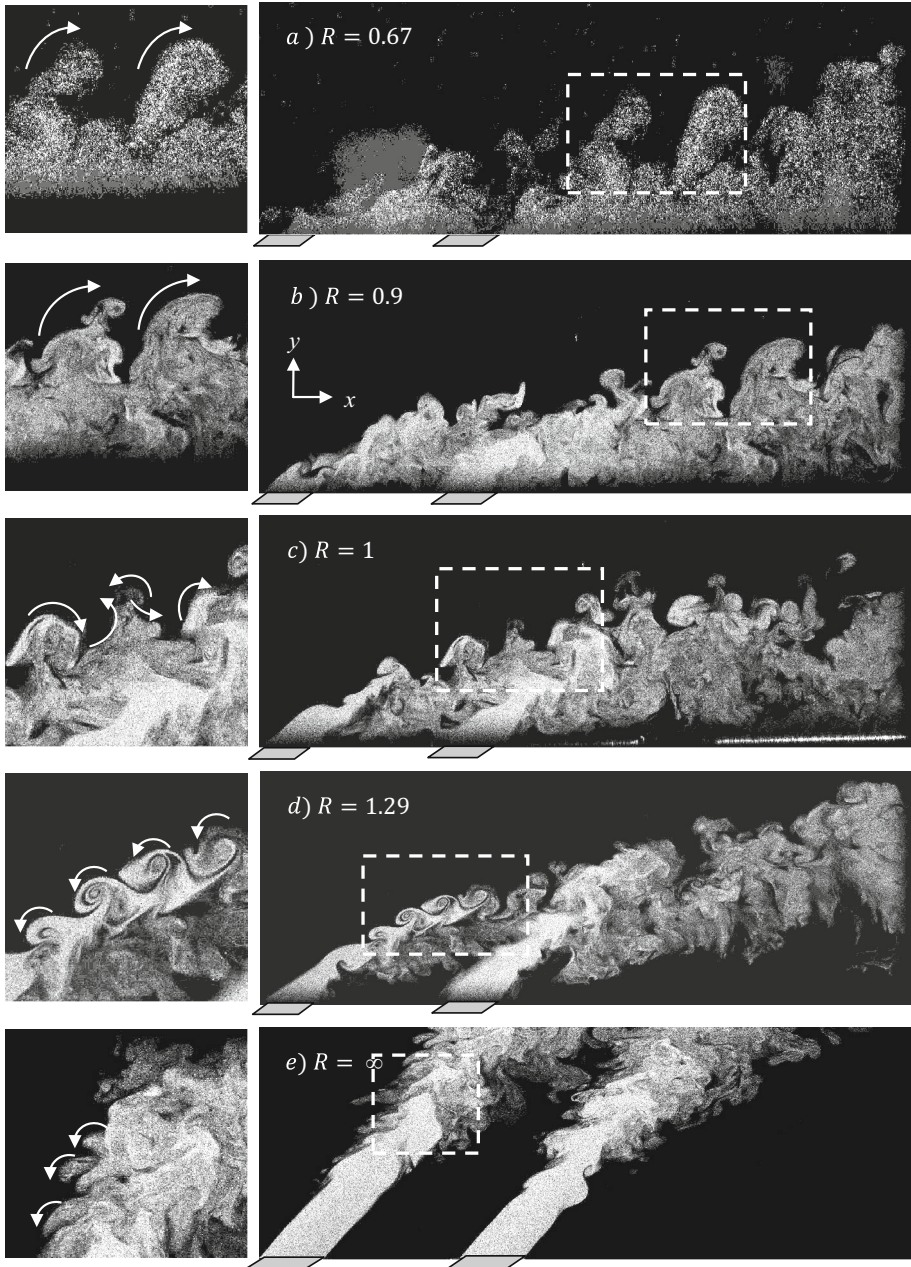


Fig. 5 Effect of the injection ratio over the CCD images taken at the symmetry plane ($z = 0$). **a** $R = 0.67$, **b** $R = 0.9$, **c** $R = 1$, **d** $R = 1.29$, **e** $R = \infty$

- the total number of flow fields used to compute time averages and root means square (rms)
- the development of reverse flows and the deformation of the flow within target areas which may deteriorate the algorithm correlations
- excessive velocity gradients and out-of boundary particle motion
- the projection of tridimensional arrows into bi-dimensional ones

In addition to these factors, problems associated with particle image overlap, non-uniform illumination of the sample volume, reflections of surfaces, particle coalescence, non-uniform flow seeding and image discretization all contribute to the number of correlation anomalies. These problems, although not as serious as velocity gradient and out-of boundary effects, contribute to sub-pixel bias errors and are often the cause of spurious vectors [35]. The uncertainties of the experiments in the present study did not exceed 5 %.

3 Results and discussion

As previously stated, our main objective is to evaluate the impact of two major parameters, namely the injection ratio and height. In a first step, we propose to track the development of the resulting flowfield of the twin inclined jets in crossflow under a variable injection ratio. After the main structures are observed and characterized in each injection case, we proceed to exploring the effect of the injection height and subsequently try to compare it and relate it to that of the injection ratio.

3.1 Effect of the flow regime on resulting flowfield structures

Figure 5 presents CCD images depicted on the symmetry plane ($z = 0$) under different flow regimes. The flow regimes are determined by the injection ratio and defined by jets to crossflow velocities. Five values were considered: 0.67, 0.9, 1, 1.29 and ∞ . The latter case corresponds to free inclined jets, and was considered to determine the effect of the presence of the crossflow.

The above mentioned injection ratio values may be divided into three categories: less than, equal to or higher than one, corresponding to jets weaker, equivalent to or stronger than the crossflow in terms of dynamic “strength”. Emphasis is particularly put on the different progress stages of the emerging jets within the surrounding crossflow and the corresponding induced vortical structures: type, size, location and orientation.

Under the weakest injection ratio, $R = 0.67$, corresponding to jet and mainstream Reynolds numbers respectively equivalent to 3591 and 9.3×10^4 , jets are closer to the injection ground. Herrin, we would like to highlight that Reynolds number was defined as follows: $Re = \frac{\rho U D_H}{\mu}$, where $D_H = 4S/P$ is the hydraulic diameter, S the section and P the perimeter of the discharging cross section, and U the mean velocity over the discharging section. Reynolds number was calculated at 20 °C, which corresponds to a density and dynamic viscosity respectively equivalent to $\rho(\text{air}) = 1.2 \text{ kg m}^{-3}$ and $\mu = 1.8 \times 10^{-5} \text{ Pi}$.

In fact, the injection ratio corresponds to the jets to mainstream velocities ratio. The weakest ratio represents then the slightest impact of the jets towards the incoming crossflow, making them consistently tilted and even flattened against the injection ground. This flattening results in clockwise rotating vortices clearly illustrated on the upper periphery of the jets in the corresponding zoomed view (Fig. 5a). When $R = 0.9$, jets are still “weaker”

then the oncoming crossflow, although their dynamic strength is getting closer to the mainstream’s one, bringing about consistent interactions. Smaller ratios on the contrary induce a less dominant rotation sense of the induced vortices. In fact, a zoom over the

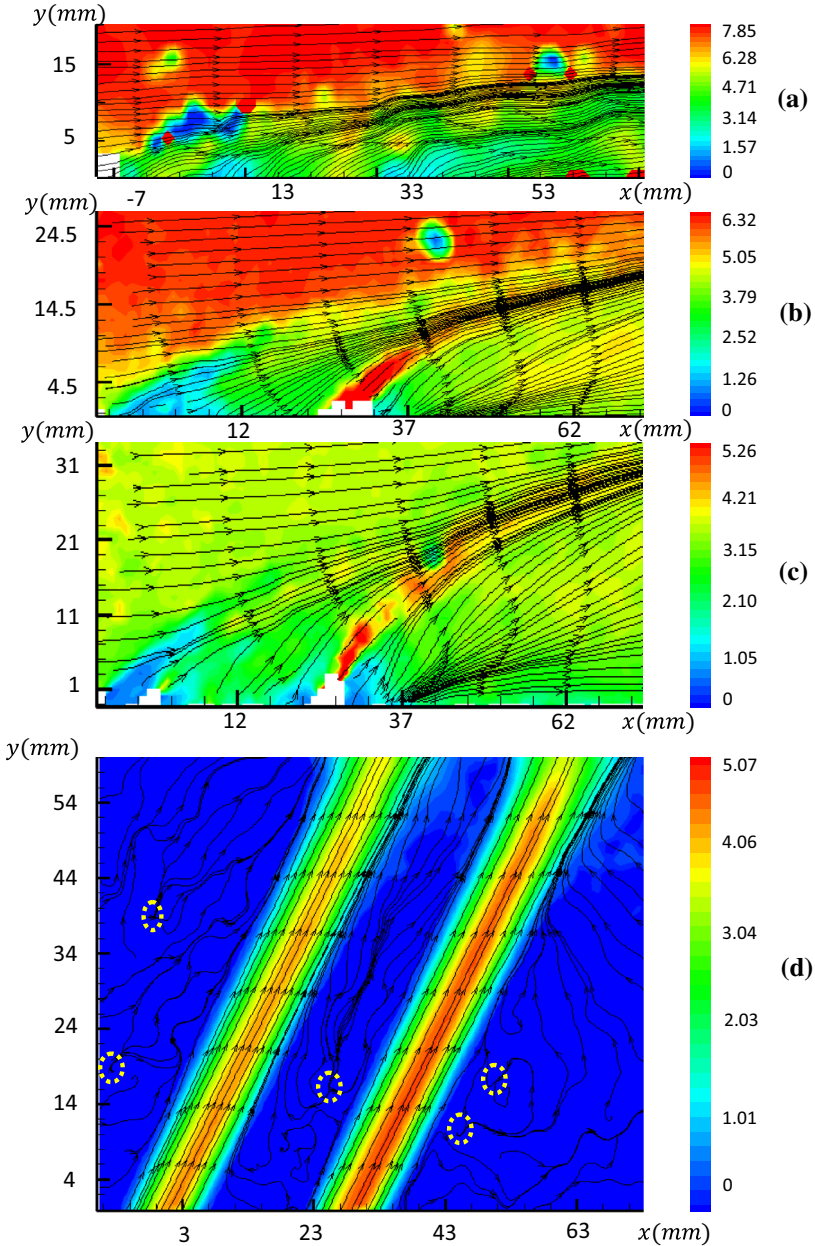


Fig. 6 Mean velocity (in m/s) cartographies on the symmetry plane and under the different velocity ratios. **a** $R = 0.67$, **b** $R = 1$, **c** $R = 1.29$, **d** $R = \infty$

upper periphery of the jets (Fig. 5b) still reveals a clockwise rotation of the vortices with the emergence of subdued embedded opposite vortices. When we reach $R = 1$, corresponding to jet and mainstream Reynolds numbers respectively equivalent to 4292 and 8×10^4 , these vortices take their full consistency and compete with the clockwise vortices as both interacting flows detain similar “consistency” and confront each other similarly, which justifies the coexistence of both types of vortices (Fig. 5c). When $R = 1.29$, corresponding to jet and mainstream Reynolds numbers respectively equivalent to 3233 and 4.6×10^4 , anticlockwise rotating vortices settle down and are particularly outstanding over the upper periphery of the emerging jets (Fig. 5d). The case considered in the absence of crossflow still reveals some anticlockwise rotating vortices even though they are no longer so outstanding (Fig. 5e). Actually, there are no more interactions between the jets and the oncoming crossflow due to the absence of the crossflow. We rather notice a simple emergence of a double jet within a stagnant surrounding flow, or an extremely slow crossflow. This mechanism is at the origin of the confusingly-shaped vortices over the jets’ periphery, commonly referred to as shear layer, leading edge or ring like vortices [16, 17, 19].

In addition to changing the sense of rotation of the ring vortices, increasing the injection ratio reduces jet-to-jet interaction. In fact, the jets are bound to tilt and flatten against the injection ground under small ratios, concentrating them close to it, and then leading to a consistent confrontation between both of them initially and between them and the injection ground later on.

This mechanism, commonly known as reattachment, is particularly remarkable under small injection ratios and results in particular vortices, called wake, upright, zipper, tornado-like, or Fric’s vortices [16–18] in acknowledgment of Fric and Roshko who first identified them by means of smoke wire visualization [36]. As the injection ratio rises, the jets have more impact on the crossflow as they cross it deeper (weaker bending effect). At the highest injection ratio (Fig. 5e), we even note almost free jets that barely interact and only far from the injection ground when they expand far enough within the surrounding flow, even if stagnant ($R = \infty$). Wake vortices are also affected far downstream of both jets, where they reattach increasingly less with increasing injection ratios. In fact, “stronger” jets are sent farther from the injection ground, and then are less forced to flatten against it and interact with it. On the contrary, under the smallest injection ratio (Fig. 5a), we barely distinguish each of the jets’ progression as they almost remain flush to the ground.

Subsequently, we notice that an increasing injection ratio helps strengthen the emitted jets with reference to the oncoming crossflow; thus reducing their flattening against the injection ground and the associated reattachment mechanism. The vortices developing on the upper periphery of the jets, commonly called the ring-like or shear vortices, consequently undergo a change in their rotation direction from clockwise to anticlockwise.

In the following, we undertake to account for the consequences of such an increasing of the injection rate on the dynamics of the interacting flow by considering Fig. 6, where the contours of the mean velocity over the same symmetry plane ($z = 0$) and under the same injection ratio, 0.67, 1, 1.29 and ∞ . Streamlines were joint to the mean velocity contours in order to highlight the variations brought to the flow structures as well.

Two main features stand out from this figure and strongly sustain the already depicted observations. Jets under the smallest injection ratio, $R = 0.67$, are rapidly and consistently tilted and flattened, bringing the streamlines closer downstream of both jets, and a wake area develops close to the ground (Fig. 6a). As the injection ratio rises, the jets are sent farther among the domain and undergo a less flattening effect demonstrated by quasi-parallel streamlines, and stemming from the emitting jet nozzles (Fig. 6d). Elsewhere, the

flow slows down till becoming stagnant under the infinite injection ratio. The stagnation of the flow is highlighted by means of the nodes in the streamlines encircled in Fig. 6d.

3.2 Impact of the injection height on the resulting flowfield

In the following, we propose to examine the impact of the injection height on the jets' progression. This evaluation is carried out as previously, in terms of the resulting flowfield structures, illustrated in the CCD images shown in Fig. 7. Injection height varied between the above mentioned values, namely $h = 0, 1, 2$ and 5 cm. In addition, consideration was given to different flow regimes (different injection ratios), apart from the free jets' case, to get a comprehensive idea about the behavior of the resulting flowfield. Such a procedure aims at comparing the effects of both parameters, qualitatively and quantitatively. Figure 7 reproduces the observations made about Fig. 5, though restrained to defined injection ratios, and tries to test them under different injection heights. We clearly witness a decreasing reattachment of the discharged jets to the ground under increasing injection rates (going from left to right). It also sustains the shift in the rotation direction of the shear layer vortices, from clockwise to anti-clockwise, at least majorly.

These observations are further sustained as we examine the figure from top to bottom, with increasing injection heights. When considering Fig. 7I-a for example, we see how rapidly and consistently flattened are the jets when sent flush to the ground under the smallest injection ratio ($R = 0.67$), leading to a remarkable wake area both between the jet columns (encircled zone) and downstream of them (indicated by the blue bold arrows).

Sending the jets at a higher level from the ground sends them farther within the domain, leading to progressively reduced wake areas. This is demonstrated by a smaller encircled

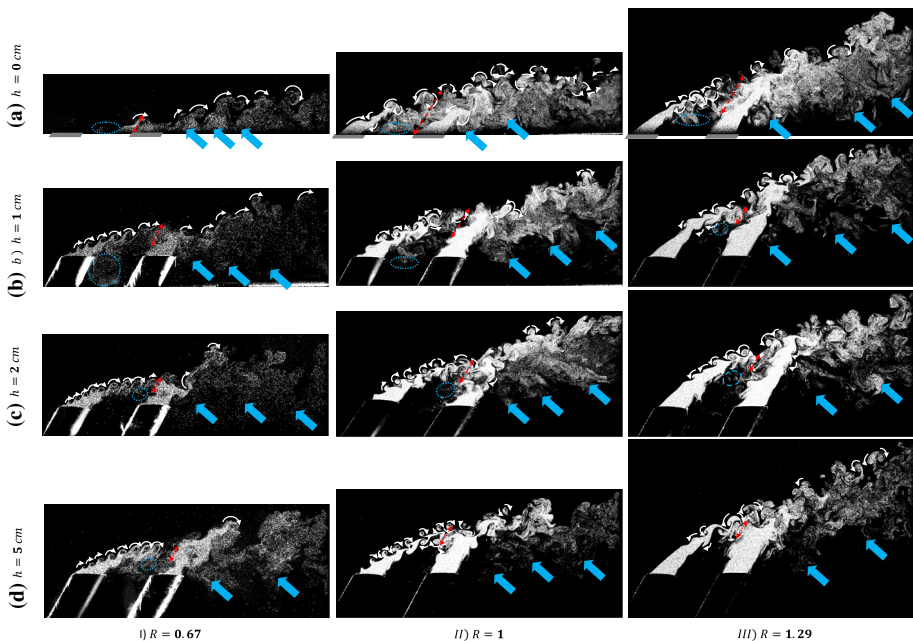


Fig. 7 Impact of the injection height on the resulting flowfield induced vortices under different regimes

zone between the jet columns and by a plume that declines farther (from the ground) and less consistently far downstream. It consequently spreads the least under the highest injection height (Fig. 7I-d). The rotation direction of the vortices developing at the upper periphery of the jets, however, remains almost the same, indicating that this feature depends only on the flow regime.

Similar observations are depicted under the following ratios ($R = 1$ and 1.29) as the jets reattach less to the ground while keeping a quasi-constant rotating direction of the ring-like vortices (Fig. 7II, III).

We also notice that the effects of the injection ratio and the injection height are complementary. In fact, increasing both parameters helps strengthen the jets and send them farther within the domain, giving rise to a much weaker wake area or even its complete absence as no plume is observed at higher levels (fig.III-c and d). Between the discharging nozzles, the jets look more like columns that interact at a progressively higher level, and their interaction tends towards a combination rather than a confrontation.

Herein, we would like to stress the fact that the complementarity of the impact of the injection ratio and height, concerns only the straightening of the jets. On the contrary, it practically does not affect the rotation direction of the vortices induced over their periphery. In fact, under a small injection ratio, the ring-like vortices develop almost over all the upper periphery of the jet plumes, while under the highest one, the rotation direction of these vortices is rather distinct in the rear zone, i.e. before the joining of the emerging jets (Fig. 7 from I to III). Similarly, the rotation direction of the ring-like vortices is less distinct as the jets are discharged at a higher level (Fig. 7 from a–d).

Now that we have considered the impact of the injection height over the global resulting flowfield behavior, we propose to extend our study to the behavior of the slightest structures of the interacting flows. For this matter, we propose to track the development of the streamlines of the resulting flowfield in Fig. 8 within the symmetry plane ($z = 0$), still under the different flow regimes ($R = 0.67, 1$ and 1.29).

For a given injection ratio, $R = 0.67$ for example, we clearly detect the straightening of the jets when discharged at a higher level from the ground; this is demonstrated by the

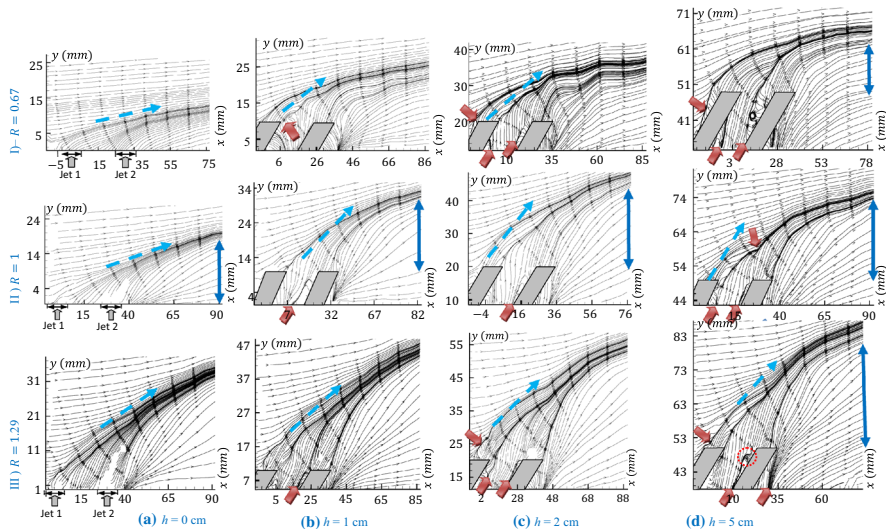


Fig. 8 Effect of the injection height and ratio over the streamlines depicted on the symmetry plane ($z = 0$)

progressively less inclined dashed blue arrow (Fig. 8I). The same phenomenon is observed under the following flow regimes even though less consistently. In fact, when sent at a higher level, the jets are sent farther before being flattened. Since discharging the jets under increasing injection ratios straightens them further, both effects are combined to give rise to generally more straightened jets. This is demonstrated by less straightening dashed blue arrows in Fig. 8 from left to right (Fig. 8a–d) and from top to bottom (Fig. 8I–III).

We also note a higher rise of the merged plumes when the jets are sent both at a higher level from the ground and under a higher injection ratio. The plume rise is a technical term already used by MacDonalds et al. [6] and Anfossi et al. [10]. It accounts for the elevation of the combined plumes of both jets. In our case, the merged plume, indicated in Fig. 8 by vertical continuous blue arrows, is measured with reference to the level of the nozzles' discharging cross-section. Herein, we would like to highlight that the rise of the merged plumes is measured at a constant distance from both jet nozzles, namely almost 50 mm from the downstream nozzle in Fig. 8. The rise of the merged plumes is higher both under increasing injection height and ratio. This is a direct consequence of the jets' straightening as mentioned earlier.

Further observations concerning the stagnated zones can be made. They are demonstrated by the nodes and bifurcation lines detected over the evolving streamlines. Indicated within the dashed arrows, they seem to be more abundant and clearer when the jets are sent from higher levels from the ground (Fig. 8d). They actually develop against the walls of the injection nozzles, and are naturally more important under higher injection levels. Similar observations were recorded in the case of single jets in crossflow by Huang and Hsieh [37, 38], Hassan and Kelso [25] and Cutler and Kelso [26]. However, for all cases, we cannot clearly distinguish the features they talked about, namely the source point, the jet-wake bifurcation line and the tube-wake bifurcation line. This is due to the fact that we handle inclined double jets in crossflow while they studied single straight jets in crossflow. However, we managed to detect these features under the highest injection height and ratio case (Fig. 8III-d). The bifurcation lines indicated with red arrows separate the flowfield into reverse and forward flow areas. In fact, the bifurcation lines separate the flow entrained into the lee side of the deflected jets from the flow carried downstream by the crossflow in the near field [25, 26]. These lines join at a node, also called source point, which is encircled in the red dashed zone (Fig. 8III-d). The flows emitting from the source point are coming from the lateral flows, which originate from the recirculation bubbles formed when the crossflow passes over the tube of the jet [37, 38]. Here we rather observe a source point originating from the crossflow coming over both tube jets, leading the flow to be trapped between both jet columns and the ground. Downstream of the second jet nozzle, no more nodes develop due to the weaker developed recirculation zone, which is probably due to the weaker crossflow reaching the zone. In fact, the recirculation bubble in the wake is generally induced by the interaction of the downwash effect of the oncoming crossflow passing over the tube tip and the up-shear effect of the jet flows [37, 38]. In the present case study, we have a more visible up-shear effect since we are dealing with two jets instead of a single one. This mechanism results in a much weaker recirculation bubble if not a stagnant zone as we already discussed in Fig. 6.

For a further and deeper processing of the resulting flowfield, we propose to focus on each of the jets' behaviors, still under the same parameters' variation, namely the injection height and ratio. For this end, we consider in Fig. 9 the development of each of the jets' trajectories by tracking the development of the streamlines issuing from the centre of each of the jet nozzles' cross-sections. The jet trajectories are then superposed for a better comparison in terms of ascension, expansion and bending.

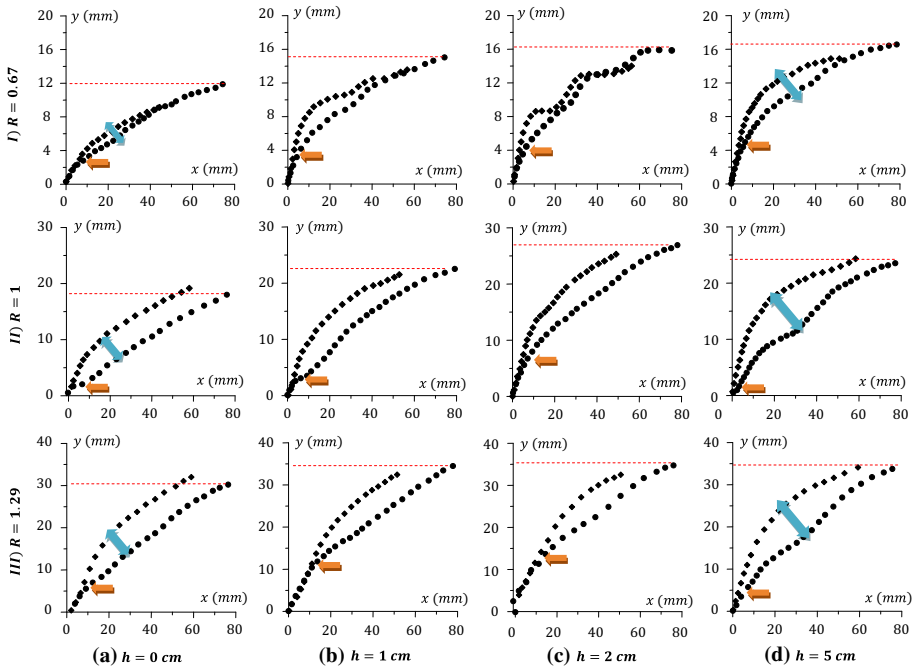


Fig. 9 Effect of the injection height over of the progression of the central core of both jets under different regimes on the symmetry plane ($z = 0$) filled circle 1st jet, filled diamond 2nd jet

The dashed red lines in the figure (Fig. 9) point out the vertical level reached by the rear jet plume after interaction with the surrounding crossflow. Under weak velocity ratios, the jets are confronted with a consistent mainstream preventing them from going too far (from the level of the discharging cross-section) before being flattened. This mechanism is reinforced by the reattachment to the ground once the jets are sent flush to it, which justifies the quickest bending of the jets (Fig. 9I-a). On the contrary, the jets are progressively bent under the highest injection ratio and height and sent the farthest (Fig. 9III-d) due to the further impulse given to the jets, to deeper cross the surrounding mainstream and cancel the attaching reattachment mechanism to the ground. Both jets undergo this effect; although it is more effective on the rear jet (the first one). In fact, due to its prior location, the rear jet faces directly and more consistently the crossflow. The flattening mechanism is fully performed, regardless of its amplitude. As to the second jet, it is “shielded” from a direct and then consistent confrontation and bending thanks to its downstream location, which allows it to cross deeper the mainstream before being caught (interrupted) by the flattening effect. This is illustrated in the Fig. 9 by the non-coincidence of both jets’ trajectories. It is to mention that the jets coincide first over a slight distance that increases with the injection height (indicated by the higher level of the orange arrow). In fact, sending the jets from a higher level cancels the reattachment effect, enabling them to cross deeper the domain before undergoing the crossflow’s deflection effect. When comes the turn of the second jet, it bends too but less consistently thereby justifying the separation between the jet trajectories. This separation indicated by the double-sided blue arrow is of course more important under higher injection levels and ratios as well (Fig. 9III-d) due to the complementarity of both parameters.

Now, let's have a closer look at the impact of the injection height over each of the jet trajectories, separately, and under all considered flow regimes.

The previous observations are confirmed in Fig. 10. Under all flow regimes, we progressively notice less flattened jet trajectories when sent at a higher level and under a higher injection ratio; this is of course valid for both jet trajectories.

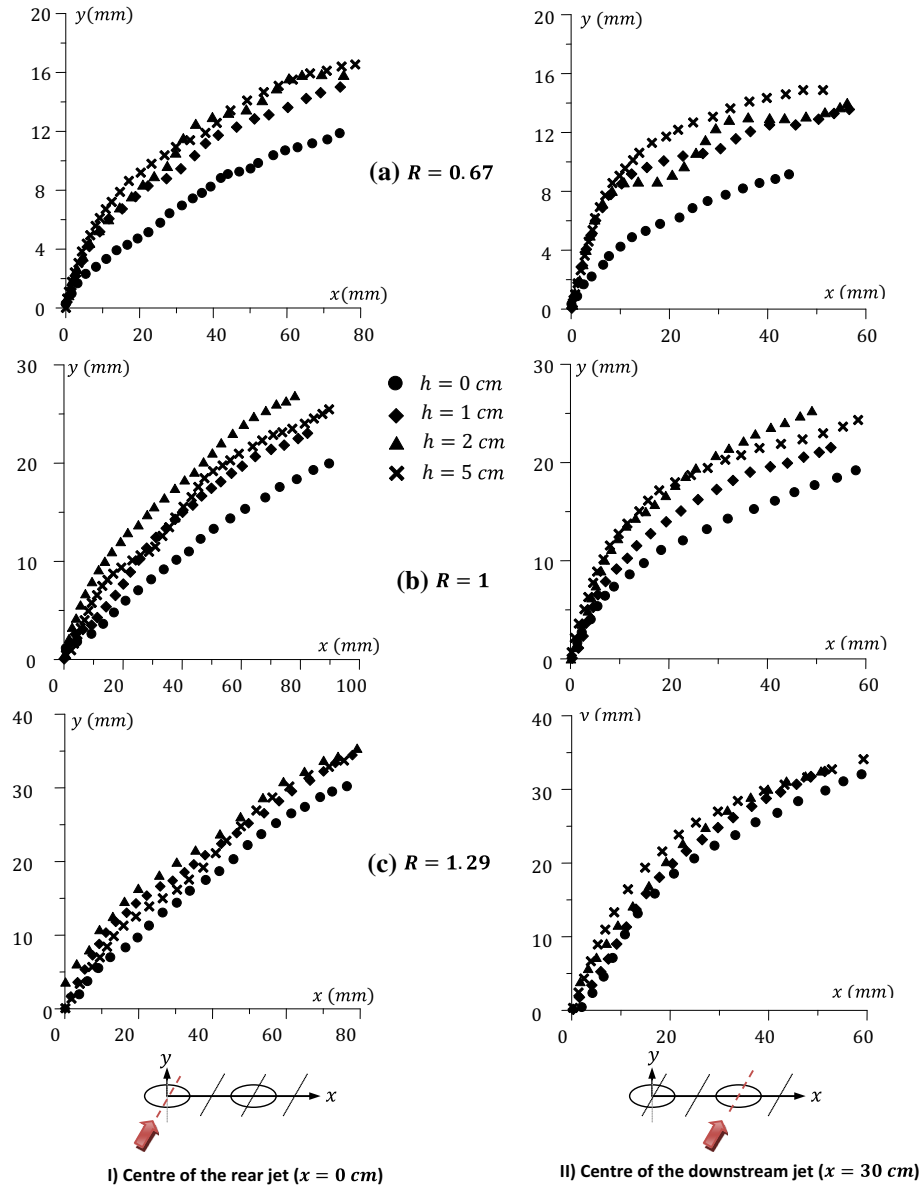


Fig. 10 Effect of the injection height over each of the jets' central cores progression in the symmetry plane ($z = 0$) under the different flow regimes

We also note the consistent separation between the ground and elevated jet trajectories. This separation fades with the injection ratio (Fig. 10I) but is reinforced in the case of the downstream jet (Fig. 10II). The separation distance fades away due to the complementarity of the injection height and ratio while it becomes more ostensible between the first and second jet trajectories due to the interference of an additional parameter, namely the shielding provided by the rear jet.

Herein, we cannot avoid mentioning some irregularities observed in Fig. 10I-b, where sending the jets at a higher level does not automatically result in a straightened rear jet. This irregularity may be justified by the critical value of the injection ratio ($R = 1$) since as we already said we are in presence of interacting jets with “similar” crossing abilities.

Figure 11 presents the evolution of the longitudinal velocity component in the symmetry plan ($z = 0$) in four representative longitudinal locations. The locations are placed within the centre of both jet nozzles’ cross-sections ($x = 0$ and 30 mm), at mid distance between them ($x = 15$ mm) and a mid distance downstream of the second jet nozzle ($x = 45$ mm) as indicated in the bottom of the figure.

It is interesting to note the presence of a single velocity peak when placed within the centre of the rear jet nozzle (Fig. 11a). This peak is reached farther from the level of the nozzles’ cross-section when the injection ratio increases. This is due to the further impulse given to the discharged jet to cross deeper the domain before being tilted. Since the flattening is delayed, the velocity peak is reached over a longer distance, postponing the jet mixing within the surrounding mainstream. Since the injection height plays a complementary role to that of the injection ratio, sending the jet from a higher level from the ground also delays reaching the velocity maximum. This delay is illustrated by the superposition order of the different plots and the slower decreasing gap between the plotted profiles. The different velocity profiles are more remarkable under the slightest injection

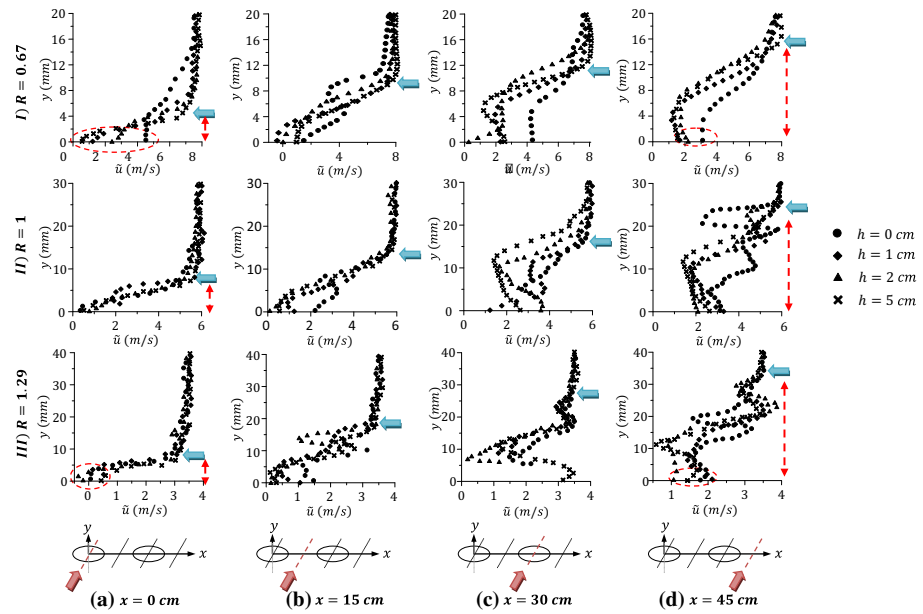


Fig. 11 Effect of the injection height over the vertical development of the longitudinal velocity within the symmetry plane ($z = 0$) at specific longitudinal locations ($x = cte$)

ratio (Fig. 11I-a), and the distribution of the jet discharged flush to the ground is the farthest due to its consistent flattening (both weak injection height and ratio). The jet is, therefore, consistently oriented towards the longitudinal direction.

Herein, we have to note the different initial values of the longitudinal velocity component in spite of the similarity of the initial conditions of jet discharge. This may be explained by the fact that the higher the jet is discharged, the farther it is sent, and the more its upstream side is affected by the crossflow. This location is actually the shelter of the horseshoe vortices, described in the literature [39] to take place when the main flow fluid is deflected laterally from the center plane due to the adverse pressure gradient in front of the jet. The spanwise vorticity in the boundary layer is then stretched to form the front of the horseshoe vortices. The latter are actually induced by the adverse pressure gradient, formed at the injection wall that forces the wall boundary layer to separate.

Since sending the jet at a higher level from the ground helps the jet cross the mainstream more deeply, it is also at the origin of a higher pressure gradient between the main flow and the one discharging from the jet nozzle. This higher pressure difference is likely to induce the mainstream to be more consistently aspirated by the emitting jet nozzle, and thus affecting the initial value of the longitudinal velocity at the centre of the nozzle's cross-section.

Increasing the injection ratio decreases the overall velocity values. It becomes even negative under the highest injection ratio and an injection height of $h = 2$ cm (Fig. 11III-a). This may be explained by the rapidity of the jet crossing the mainstream leading to an even further pressure gradient and then more main flow aspiration that may generate a reverse flow.

Within the second jet location (Fig. 11c), two peaks are reached. The first one is relative to the just emitted second jet while the second one is relative to the expanded rear jet plume. Similarly to the peaks registered within the rear jet location, the ones attained here are more distinct under the weakest injection ratio and height, to get closer when both parameters rise. However, they get closer under a greater injection ratio with reference to what happens within the 1st jet location which is probably due to the shielding effect provided by the rear jet plume. Herein, it is interesting to see the higher gap between both maxima (velocity peaks) and the minimum registered velocity component. The latter vanishes under the $h = 2$ cm both under the highest and weakest injection ratios which is probably due to the upward bifurcation line that shields the stagnant flow.

Far downstream of both jet nozzles, the profiles are more regular under the weakest injection ratio since the jets have already undergone the most tricking interactions. Under higher ratios, the jets still are consistent and reach farther downstream locations, justifying the more elaborate variations along the velocity distributions. An interesting decrease in the longitudinal velocity component is observed and more particularly under the $h = 2$ and 5 cm. Under those injection height cases, the jets penetrate further the domain, and so do their combination. They consequently stand longer and farther than under the weaker injection height cases, justifying the higher (even slightly) peaks, and leading to a consistent wake region under their leeward edge. The wake region tends even to shield a stagnant flow under $h = 5$ cm since velocity seems to vanish in the vicinity of $y = 11$ cm (Fig. 11d-III).

4 Conclusion

The present experimental study examined twin aligned jets in crossflow model. Jets were sent both flush to the ground and at different injection height levels, in an attempt to evaluate the resulting flowfield behavior. Experiments were carried out by means of particle image velocimetry (PIV) technique under different flow regimes. The major focus was laid on the induced vortical structures and to the evolution of the discharged jets within the oncoming crossflow, in terms of streamlines and velocity distributions, within the symmetry plane ($z = 0$).

The injection height and ratio play a complementary role and provide the jets with further penetration before being tilted and flattened; then, leading the jets to follow higher trajectories as already proved by Cutler and Kelso [26] and Hassan and Kelso [25] in the case of a single jet in crossflow.

In addition to changing the sense of rotation of the ring vortices, increasing the injection ratio reduces jet-to-jet interaction, which seriously reduces their flattening against the injection ground and the associated reattachment mechanism. However, the complementarity of the injection ratio and height concern only the jet-to-jet interaction and not their individual rotation direction, especially at their periphery.

The wake of the jets witnesses a much weaker recirculation bubble if not a stagnant zone under increasing higher injection ratios and heights due to the weaker reattachment mechanism to the ground. Both jets undergo this effect; although it is more effective on the rear jet (the first one).

Further experiments are certainly to be carried out if not extended by numerical simulation to investigate further these observations and extend them. The streamwise direction is also to be considered to get a deeper insight into the most dominant vortical structure established, namely the CVP, as well as on the horseshoe vortices that develop at the basis of the discharging jet nozzles.

References

1. Lefebvre AH (1998) Gas turbine combustion, 2nd edn. Taylor & Francis, Washington, pp 324–363
2. Ibrahim IM, Gutmark EJ (2006) Dynamics of single and twin circular jets in crossflow. 44th AIAA 2006-1281 Aerospace Sciences Meeting and Exhibit, Reno, Nevada
3. Ziegler H, Wooler PT (1971) Multiple jets exhausted into a crossflow. *J Aircr* 8(6):414–420
4. Ziegler H, Wooler PT (1973) Analysis of stratified and closely spaced jets exhausting into a crossflow. National Aeronautics and Space Administration, Washington
5. Gregoric M, Davis LR, Bushnell DJ (1982) An experimental investigation of merging buoyant jets in a crossflow. *ASME J Heat Transfer* 104(2):236–240
6. Macdonald RW, Strom RK, Slawson PR (2002) Water flume study of the enhancement of buoyant rise in pairs of merging plumes. *Atmos Environ* 36:4603–4615
7. Contini D, Robins A (2004) Experiments on the rise and mixing in neutral crossflow of plumes from two identical sources for different wind directions. *Atmos Environ* 38:3573–3583
8. Contini D, Hayden P, Robins A (2006) Concentration field and turbulent fluxes during the mixing of two buoyant plumes. *Atmos Environ* 40:7842–7857
9. Kolar V, Savory E (2007) Dominant flow features of twin jets and plumes in crossflow. *J Wind Eng Ind Aerodyn* 95:1199–1215
10. Anfossi D, Bonino G, Bossa F, Richiardone R (1978) Plume rise from multiple sources: a new model. *Atmos Environ* 12:1821–1826
11. Gangoliti G, Sancho J, Ibarra G, Alonso L, García JA, Navazo M, Durana N, Ildardia JL (1997) Rise of moist plumes from tall stacks in turbulent and stratified atmospheres. *Atmos Environ* 31(2):253–269

12. Bunsirisert K, Orrala C, Rahai HR (2005) Profiles of two elevated side-by-side turbulent jets in a crossflow. 43rd AIAA Aerospace Sciences Meeting and Exhibit, Reno, Nevada
13. Briggs GA (1974) Plume rise from multiple sources., Proceedings of cooling tower environment, University of Maryland, pp 161–179
14. Briggs GA (1975) Plume rise predictions. Lectures on Air Pollution and Environmental Impact Analyses. American Meteorological Society, pp 59–111
15. Montgomery TL, Norris WB, Thomas FW, Carpenter SB (1973) A simplified technique used to evaluate atmospheric dispersion of emissions from large plants. *J Air Pollut Control Assess* 23:388–457
16. Radhouane A, Bournot H, Said NM, Mhiri H, Le Palec G (2009) Numerical and experimental study of a double jet inclination variation on its dynamic evolution within a crossflow. *Heat Mass Transf J* 45(12):1597–1616
17. Radhouane A, Said NM, Mhiri H, Le Palec G, Bournot P (2009) Impact of the initial streamwise inclination of a double jet emitted within a cool crossflow on its temperature field and pollutants dispersion. *Heat Mass Transf J* 45(6):805–823
18. Radhouane A, Mahjoub SN, Mhiri H, Le Palec G, Bournot P (2010) Impact of the temperature gradient between twin inclined jets and an oncoming crossflow on their resulting heat transfer. *J Comput Therm Sci (CTS-1071)* 2(6):487–499
19. Radhouane A, Mahjoub Said N, Mhiri H, Le Palec G, Bournot P (2010) Dispersion of twin inclined fume jets of variable temperature within a crossflow. *Defect Diffus Forum* 297–301:936–941
20. Moor DJ (1974) A comparison of the trajectories of rising buoyant plumes with theoretical/empirical models. *Atmos Environ* 8:441–457
21. Goyal P, Rama Krishna TVBPS (2002) Dispersion of pollutants in convective low wind: a case study of Delhi. *Atmos Environ* 36:2071–2079
22. Cutler PRE (2002) On the structure and mixing of a jet in crossflow. Ph.D. Thesis, Department of Mechanical Engineering the university of Adelaide, Australia
23. Rama Krishna TVBPS, Reddy TR, Reddy MK, Singh RN (2004) Assimilative capacity and dispersion of pollutants due to industrial sources in Visakhapatnam bowl area. *Atmos Environ* 38:6775–6787
24. Stathopoulos T, Lazure L, Saathoff P, Gupta A (2004) The effect of stack height, stack location and rooftop structures on air intake contamination. A laboratory and full-scale study, R-392, IRSST
25. Hassan ER, Kelso RM (2005) Near field structure of flush-mounted and elevated transverse jets. Proceedings of the 4th Australian conference on laser diagnostics in fluid mechanics and combustion, the University of Adelaide, Australia
26. Cutler PRE, Kelso RM (2001) On the structural differences between elevated and flush-mounted transverse jets. Proceedings of the 4th Australasian Fluid Mechanics conference Adelaide University, Adelaide, Australia 10–14 December 2001
27. Olcese LE, Toselli BM (2005) Development of a model for reactive emissions from industrial stacks. *Atmos Environ* 20:1239–1250
28. Megerian S, Davitian J, De B Alvares LS, Karagozian AR (2007) Transverse jet shear layer instabilities. Part 1: experimental studies. *J Fluid Mech* 593:93–129
29. Koklu M, Baysal O (2008) Modelling, parametrization and simulation-based optimisation of a microflow-control actuator. *Int J comput Fluid Dyn* 22(6):367–381
30. Karagozian AR (2010) Transverse jets and their control. *Prog Energy Combust Sci* 36(5):531–553
31. Smith SH, Mungal MG (1998) Mixing, structure and scaling of the jet in crossflow. *J Fluid Mech* 357:83–122
32. Muppidi S, Mahesh K (2006) Two-dimensional model problem to explain counter-rotating vortex pair formation in a transverse jet. *Phys Fluids J* 18(8):085103
33. Yuan LL, Street RL (1998) Trajectory and entrainment of a round jet in crossflow. *Phys Fluids* 10(9):2323–2335
34. Jovanovic MB (2006) Film cooling through imperfect holes. Ph.D., Technische universiteit Eindhoven
35. Hart DH (1998) The elimination of correlation errors in PIV processing. Proceedings of the 9th International symposium on applications of laser techniques to fluid mechanics, Lisbon, Portugal, p 8
36. Fric TF, Roshko A (1994) Vortical structure in the wake of a transverse jet. *J Fluid Mech* 279:1–47
37. Huang RF, Hsieh RH (2002) An experimental study of elevated round jets deflected in a crosswind. *Exp Therm Fluid Sci* 27:77–86
38. Huang RF, Hsieh RH (2003) Flow visualization and LDV measurement on near-wake of elevated jets in crossflow. Proceedings of PSFVIP-4, F4101, June 3–5, 2003, Chamonix, France
39. Andreopoulos J, Rodi W (1984) Experimental investigation of jets in a crossflow. *J Fluid Mech* 138:93–127